Paleoceanography and Paleoclimatology

RESEARCH ARTICLE
10.1029/2020PA004207

Key Points:

- Molybdenum-based nitrogen fixation was prevalent in the northern European epicontinental shelf during the Toarcian carbon isotope excursion
- Quantitative denitrification and/or anammox caused nitrogen famine in strongly redox-stratified environments during the early Toarcian
- Oxygen-deficient basins on the northern European epicontinental shelf across the Toarcian carbon isotope excursion

Correspondence to:
Y. Wang,
yunfeng.wang@uni-tuebingen.de

Citation:
Wang, Y., Ossa, F. O., Spangenberg, J. E., Wille, M., & Schoenberg, R. (2021). Restricted oxygen-deficient basins on the Northern European epicontinental shelf across the Toarcian carbon isotope excursion interval. *Paleoceanography and Paleoclimatology*, *36*, e2020PA004207. https://doi.org/10.1029/2020PA004207

Received 25 DEC 2020
Accepted 18 MAY 2021

Restricted Oxygen-Deficient Basins on the Northern European Epicontinental Shelf Across the Toarcian Carbon Isotope Excursion Interval

Yunfeng Wang[1], Frantz Ossa Ossa[1,2], Jorge E. Spangenberg[3], Martin Wille[4], and Ronny Schoenberg[1,2]

[1]Department of Geosciences, University of Tuebingen, Tuebingen, Germany, [2]Department of Geology, University of Johannesburg, Johannesburg, South Africa, [3]Institute of Earth Surface Dynamics, University of Lausanne, Lausanne, Switzerland, [4]Institute of Geological Sciences, University of Bern, Bern, Switzerland

Abstract The worldwide recognition of the Toarcian carbon isotope excursion (T-CIE) in organic-rich sedimentary rocks has been linked to an oceanic anoxic event (OAE) which implies the world's deep oceans were anoxic ~183 Ma. The majority of independent redox observations used to build this argument were mainly obtained from T-CIE organic-rich sediments deposited on northern European epicontinental shelf. However, increasing evidence has shown that this shelf had limited connection with the open ocean, making it unsuitable for reconstructing the T-CIE ocean redox structure. To unveil such controversy, we present integrated $\delta^{15}N_{bulk}$ and $\delta^{15}N_{ker}$ from Dotternhausen profile, Germany, combined with literature data from other T-CIE profiles. Both $\delta^{15}N_{bulk}$ and $\delta^{15}N_{ker}$ values are predominantly between +0.3 and +2.5‰. These positive near-zero $\delta^{15}N$ values imply enhanced N_2 fixation by cyanobacteria using molybdenum (Mo)-based nitrogenase to compensate bioavailable N loss following quantitative denitrification and/or anammox in a strongly redox-stratified marine setting. Such N isotope composition contradicts the typical sedimentary $\delta^{15}N$ values (>3‰) induced by partial water-column denitrification and/or anammox in modern-ocean oxygen minimum zones. We rather propose the existence of local oxygen-deficient basins on northern European epicontinental shelf where dissolved N underwent extensive denitrification and/or anammox causing bioavailable N deficiency. Mo-based diazotrophy thus played a critical role in discriminating N isotope compositions among multiple hydrographically restricted T-CIE marginal basins. Restricted oxygen-depleted environments on the northern European epicontinental shelf unlikely represent the open-ocean redox landscape. The existence of the global OAE thus needs comprehensive redox investigations on Tethys and/or Panthalassa deep-sea T-CIE successions to validate.

1. Introduction

During the Mesozoic era, several particular periods of widespread deposition of organic-rich black shales occurred during extreme perturbations to global climate and ocean redox structure, known as Oceanic Anoxic Events (OAEs). Of these events, the early Jurassic (Toarcian) OAE at ~183 Ma is marked by a specific interval of rapid global warming (Jenkyns, 1988), second-order marine mass extinction (e.g., Harries & Little, 1999; Little & Benton, 1995) and widespread oxygen deficiency (Pearce et al., 2008), manifested in deposits of anoxic marine sediments around the globe. The Toarcian OAE also dictated a significant carbon-cycle perturbation which was along with a negative Toarcian carbon isotope excursion (T-CIE) recorded in terrestrial wood (Hesselbo et al., 2007) and marine organic- and inorganic-carbon reservoirs at a global scale (e.g., Hesselbo et al., 2000). Consequently, the global (deep) oceans were suggested to be anoxic across the T-CIE (e.g., Pearce et al., 2008; Thibault et al., 2018). The hypothesis of the suggested global deep ocean anoxia is, however, challenged by the findings that most of the Toarcian fine-grained organic-rich sedimentary successions were deposited in hydrographically restricted anoxic basins especially in the northern European epicontinental shelf region (e.g., Fantasia et al., 2018; Frimmel et al., 2004; Sælen et al., 2000), which were appreciably isolated from the open ocean (Dickson et al., 2017; McArthur, 2019; McArthur et al., 2008; Remírez & Algeo, 2020). Furthermore, contrasting redox states have been proposed for the European epicontinental shelf seas during the T-CIE, in that the development of anoxia in the bottom waters was largely limited to the northern part of the European epicontinental shelf, while the southern part remained mainly oxygenated (Ruvalcaba Baroni et al., 2018).

In this study, the biogeochemical cycle of nitrogen (N), a redox-sensitive and bio-limiting element, is used in the attempt to unravel the controversy of the Toarcian oceanic redox structure. Before the T-CIE and inferred co-evolved OAE, the oxygenated ocean is expected to have built up a large and steady nitrate (NO_3^-) reservoir. When entering the T-CIE, if sedimentary deposition occurs in open marine environments, the extensive seawater deoxygenation (OAE) would partially consume NO_3^- through water-column denitrification, the most prominent oceanic NO_3^- removal process (Sigman & Fripiat, 2019; Stüeken et al., 2016). Considering that partial denitrification and/or anammox preferentially releases ^{14}N as the form of N_2/N_2O to the atmosphere, resulting in higher $\delta^{15}N$ values of the residual N pool, organic matter (OM) deposited in open marine environment records such ^{15}N-rich seawater signal through assimilation and imparts $\delta^{15}N$ values ≥3‰ in sediments (e.g., Garvin et al., 2009; Gilleaudeau et al., 2020; Stüeken et al., 2016; Tesdal et al., 2013). This is because a large dissolved marine N reservoir is required to record the isotopic fingerprints of its redox-driven cycle in co-deposited sediments (Stüeken et al., 2016). In contrast, if hydrographic water-mass restriction represents the main depositional settings of T-CIE sedimentary rocks, quantitative denitrification and/or anammox is most likely to occur as a result of strongly redox-stratified water column (Schwark & Frimmel, 2004; Wang et al., 2020). Biomass deposited under such conditions is expected to preserve the $\delta^{15}N$ value of the main input source that is, N_2 fixation (Stüeken et al., 2016). Collectively, whether the northern European T-CIE epicontinental shelf successions were deposited in marine environments well connected to the open ocean or in very restricted environments can thus be reliably validated through evaluating the contemporaneous sedimentary N isotope records. This study reports high resolution of whole rock and separated kerogen $\delta^{15}N$ ($\delta^{15}N_{bulk}$ and $\delta^{15}N_{ker}$) data from the well-recognized T-CIE stratigraphic profile of Dotternhausen, southwestern (SW) Germany, to address the evolution of marine N biogeochemical cycling and ultimately shed new light on the expansion of anoxia in the coeval ocean.

2. Geological Background and the Studied Sedimentary Section

Early Jurassic experienced a warm period induced by a global temperature rise, reaching ~6ºC–10ºC higher than the present day (Chandler et al., 1992; Dera et al., 2011; Rosales et al., 2018; Svensen et al., 2007). This global warming event was suggested to be linked to the massively released CO_2 owing to the Karoo-Ferrar large igneous province emplacement (Pálfy & Smith, 2000; Svensen et al., 2007) and/or CH_4 released from Gondwanan organic-rich shales or methane clathrates (e.g., Hesselbo et al., 2000; Kemp et al., 2005; McElwain et al., 2005). Across the greenhouse early Jurassic (Toarcian) interval, the hydrological cycle was intensified, followed by the formation of humid climate conditions and the enhanced chemical weathering rates (Brazier et al., 2015; Cohen et al., 2004; Fantasia et al., 2018; Hermoso & Pellenard, 2014; Montero-Serrano et al., 2015; Them et al., 2017). In addition, the majority of the present-day Europe was situated on the northern European epicontinental shelf which deepened toward the southeastern part of the contemporaneous Tethys Ocean (Jenkyns, 2010) (Figure 1a). However, the northern European epicontinental shelf during the Early Toarcian was characterized by multiple isolated basins/sub-basins in which the frequency of the deep-water renewal was to some extent restricted (e.g., McArthur, 2019; McArthur et al., 2008; Röhl et al., 2001). Moreover, the warming event during the early Toarcian tied to the massive emission of the greenhouse gases (Hesselbo et al., 2000; Kemp et al., 2005; Ruebsam et al., 2019, 2020) together with the coeval large-scale tectonic activities for example, the breakup of Pangaea supercontinent, likely jointly led to seawater transgression and deoxygenation in the northwestern Tethyan shallow shelf marine areas. The pervasive deposition of the organic-rich sedimentary rocks may thus be related to the pronounced change in the paleoceanographic and paleoclimatologic conditions during the early Toarcian period (e.g., Baudin et al., 1990; Jenkyns, 2010).

The studied Dotternhausen sedimentary section (48°13′32.6″N, 8°46′29.8″E) is geographically located in the present-day SW Germany, and was deposited in the northern European epicontinental shelf seaway throughout the Early Toarcian interval (Ziegler, 1988) (Figures 1b,and 1c). This sedimentary section belongs to the well-recognized lower Toarcian Posidonia Shales that are enriched in high abundance of well-preserved OM and are widely distributed over Europe (Bour et al., 2007; Fantasia et al., 2018; Montero-Serrano et al., 2015; Song et al., 2017). A lot of previous work thus has been performed on the Posidonia Shales as case studies to understand the early Toarcian carbon cycling, continental weathering, marine deoxygenation and mass extinction (e.g., Montero-Serrano et al., 2015; Röhl et al., 2001; van Acken et al., 2019;

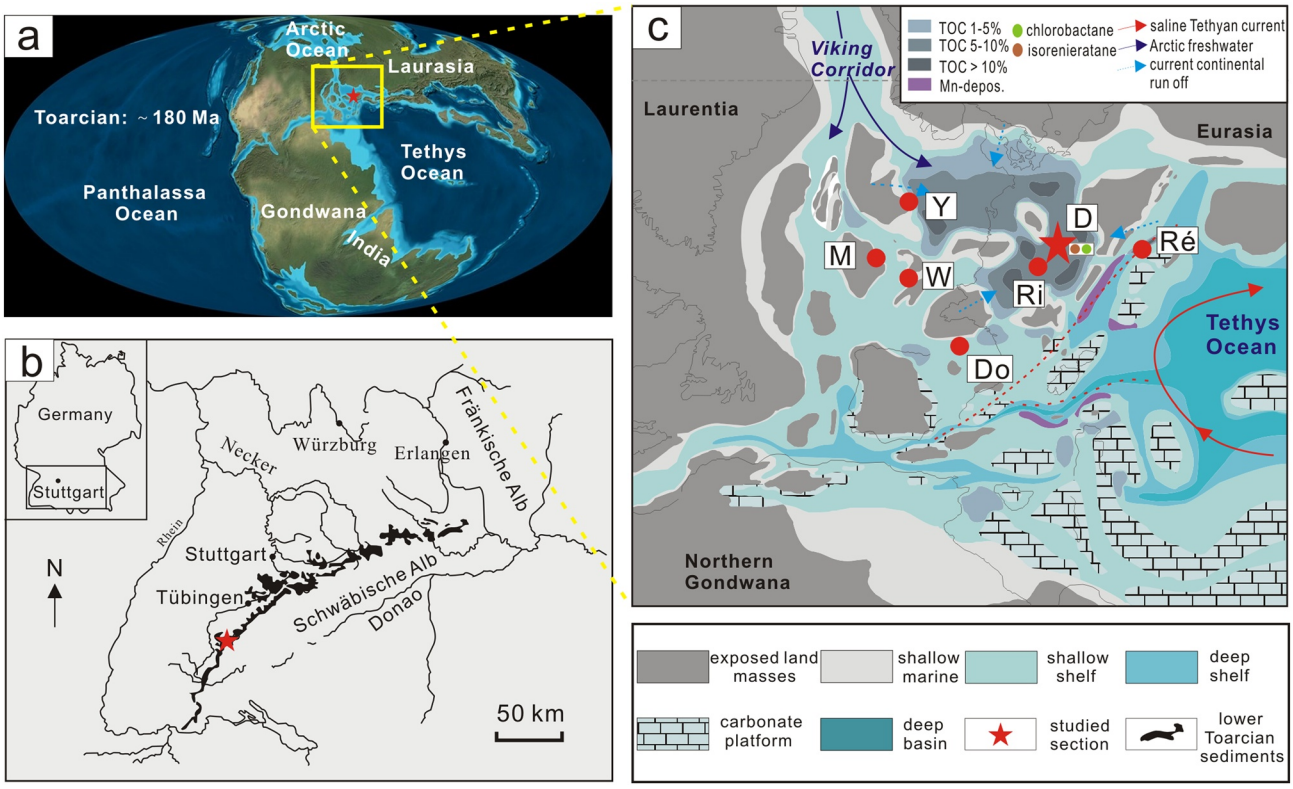

Figure 1. (a) Early Toarcian paleogeographic map with the location of Dotternhausen section (southwestern Germany). (b) Present-day map of southwestern Germany showing the site of the Dotternhausen section (modified from Röhl et al., 2001). (c) Early Toarcian paleogeography of the northern European epicontinental shelf settings (modified from Ruebsam et al., 2018). Red dots denote the Toarcian sedimentary sections spanning the CIE that are compared in this study. Dotternhausen (D; Germany), Rietheim (Ri; Switzerland), Réka Valley (Ré; Hungary), Yorkshire (Y; UK), Winterborne Kingston (W; UK), Mochras (M; UK) and Dogna (Do, Italy).

Wang et al., 2020). This Dotternhausen section has been also extensively studied and been well characterized in terms of lithostratigraphy and biostratigraphy (Röhl et al., 2001; Röhl & Schmid-Röhl, 2005). From the bottom up, this section was divided into three ammonite zones *tenuicostatum*, *falciferum* and *bifrons*, and was further subdivided into several subzones including *elegantulum*, *exaratum*, *elegans*, *falciferum*, *commune*, etc (cf. Röhl et al., 2001). In addition, three lithologic units for the Dotternhausen section have been defined in the light of the distinct abundances of the OM and siliciclastic component and different fabric types (Röhl et al., 2001; van Acken et al., 2019; Wang et al., 2020). They are bioturbated light-gray (organic-lean) shales from the depth of 1,180–980 cm, laminated fine-grained organic-rich shales and marlstones from 980–550 cm, and bituminous light-gray (organic-lean) shales from 550 to 0 cm, respectively (Röhl et al., 2001). The bioturbated light-gray shale unit starting with the limestone bed Spinatum Bank is abundant in benthic fauna and contains two intercalated thin organic-rich black shale beds (Figure 2). The fine-grained organic-rich sedimentary rocks deposited during the T-CIE are depleted in benthic fauna, and marked by high total organic carbon (TOC) concentration. These organic-rich sedimentary rocks were not metamorphosed and only experienced diagenesis in the oil window which is reflected by their persistently high hydrogen index(HI) values (580 mg hydrocarbon (HC)/g TOC on average) and their oil shale character (cf. Frimmel et al., 2004; Röhl et al., 2001; Wang et al., 2020). In the Dotternhausen section, there are three limestone beds, including the Unterer Stein, Steinplatte and Oberer Stein at the depth of ~800, ~680 and ~610 cm, respectively (Figure 2). The Unterer Stein with the thickness of 20-30 cm formed during early diagenesis and can be traced in several European countries such as Germany, Switzerland and France (van de Schootbrugge et al., 2005). It thus can be used as a stratigraphic marker to track more T-CIE sedimentary sections. The studied Dotternhausen sedimentary section has been subdivided into Aschgraue Mergel, Unterer Schiefer, and Mittlerer Schiefer Members in ascending order. The Aschgraue Mergel Member at the base of the Dotternhausen section is composed of organic-lean shales. Within the upward fine-grained

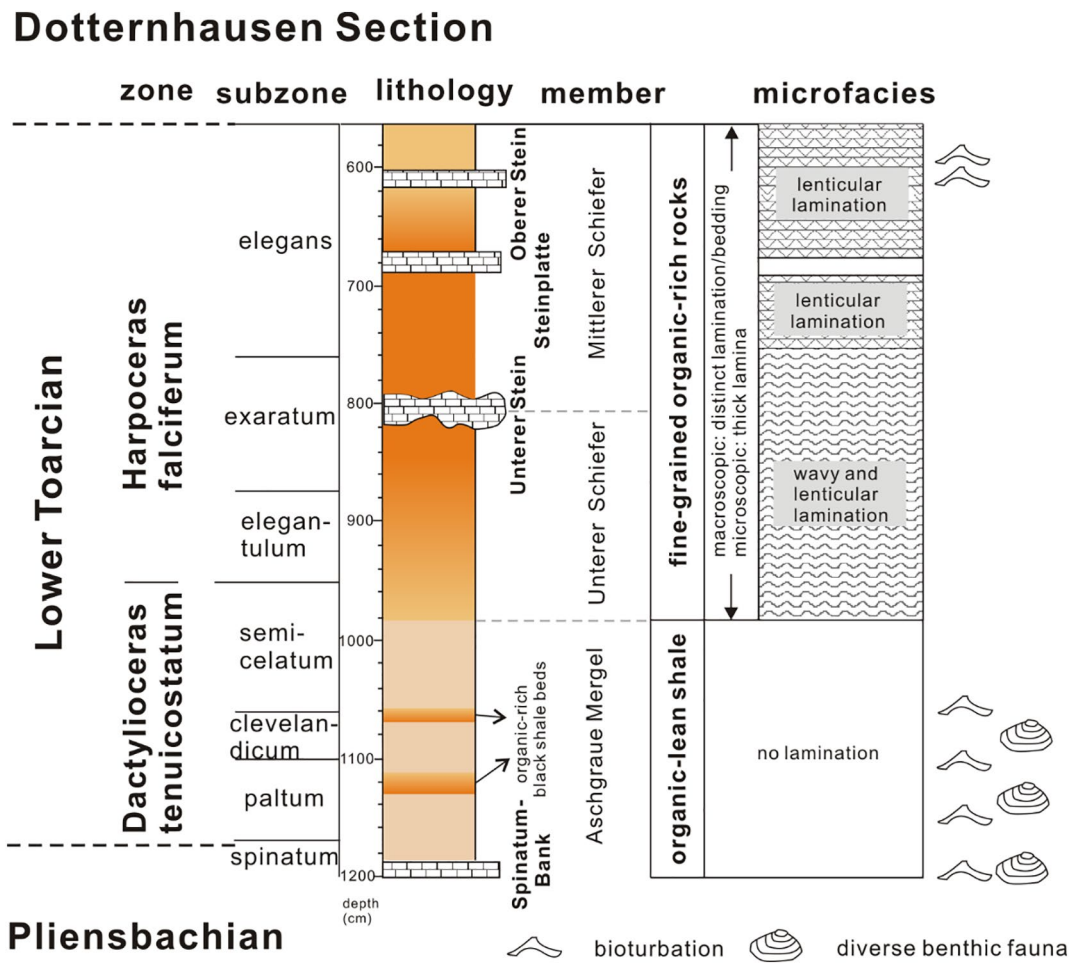

Figure 2. Stratigraphic distribution of lithology, microfacies and lamination types of the Dotternhausen sedimentary section during the Early Toarcian (modified from Röhl et al., 2001).

organic-rich rock facies, Unterer Schiefer and Mittlerer Schiefer Members are partitioned by the Unterer Stein limestone bed. A further description of the Dotternhausen sedimentary section with aspect to its paleontological and sedimentary characteristics can be found in previous studies (cf. Röhl et al., 2001; Röhl & Schmid-Röhl, 2005).

3. Materials and Methods

3.1. Sampling

In this study, the Dotternhausen sedimentary section, SW Germany, from 1,050 to 610 cm in stratigraphic depth containing the T-CIE was investigated. This stratigraphic interval starts with the upper *semicaletum* subzone and ends with the Oberer Stein in the upper *elegans* subzone (Figure 2). In detail, it comprises a lower 0.8 m-thick bioturbated light-gray (organic-lean) shale unit preceding the T-CIE and an upper 3.6 m-thick interbedded organic-rich shale and marlstone unit deposited during the T-CIE. High-resolution sampling at a small spacing (3.5 cm on average) was performed on the organic-lean shales and find-grained organic-rich sedimentary rocks from the two units in this study. A total of 31 samples were collected and used for further geochemical analyses.

3.2. Analytical Methods

To avoid potential influence from weathered materials and any handling contamination, we cut the collected sedimentary rock samples into 2 cm-thick slabs with a water-cooled saw. The slabs were cleaned and then rinsed by distilled water and analytical grade and glass distilled ethanol and dichloromethane, respectively. Following preparing the cleaned sample slabs, they were dried at 50°C for one day, and then fragmented and powdered using an agate mill. The obtained sample powders were subsequently analyzed for $\delta^{15}N_{bulk}$ and $\delta^{15}N_{ker}$, and $\delta^{13}C$ for TOC and extracted kerogen ($\delta^{13}C_{org}$ and $\delta^{13}C_{ker}$) at the laboratory of the Institute of Earth Surface Dynamics, University of Lausanne. The analytical procedure is based on the previous description provided by Spangenberg and Frimmel (2001), Spangenberg and Herlec (2006), and Spangenberg and Macko (1998).

The measurement of all C and N data was carried out by combined elemental analyzer (Carlo Erba 1,108) and isotope ratio mass spectrometry (Delta V Plus; Thermo Fisher Scientific) (EA-IRMS) under a continuous helium flow condition through a ConFlo III open split interface (cf. Spangenberg et al., 2006, 2014). For TOC, total nitrogen (TN), $\delta^{13}C_{org}$, and $\delta^{15}N_{bulk}$ analyses, powdered whole rock materials were treated by a drop-wise addition of 10% HCl to remove all inorganic carbon. For the analyses of N_{ker}, $\delta^{13}C_{ker}$, and $\delta^{15}N_{ker}$, powdered whole rock samples were gradually treated to extract the kerogen fraction that cannot be dissolved in organic solvents, non-oxidizing acids and bases. On the basis of the kerogen extraction procedure described by Durand and Nicaise (1980), this study used Soxhlet extraction method in which mixed methanol and dichloromethane were added to remove bitumen (a soluble fraction in OM), 6 M HCl was added to remove carbonate, sulfide, sulphate, and (hydro)oxide, and a mixed acid composed of 40% HF and 6 M HCl was added to remove siliciclastic fraction. These stepwise treatments were all carried out at the temperature of 65ºC–70°C, and were accelerated through using a PTFE-coated magnetic stirrer. After removing the supernatant, the residues were thoroughly washed and purified using deionized water and ultrapure water produced by Direct-Q UV3 Millipore®, respectively, and then dried at the temperature of 40°C. Following drying the solid residues, mineralogical analysis performed by a Thermo Scientific ARL X-TRA Diffractometer showed that all the silicate fraction in the whole rock samples has been removed completely.

The measured stable C and N isotope compositions are reported using delta (δ) notation in per mil relative to their standards which are Vienna Pee Dee Belemnite and atmospheric nitrogen (Air-N_2), respectively. They are thus defined as: $\delta^{13}C = (((^{13}C/^{12}C)_{sample}/(^{13}C/^{12}C)_{VPDB} - 1) \times 1{,}000$ and $\delta^{15}N = (((^{15}N/^{14}N)_{sample}/(^{15}N/^{14}N)_{Air\text{-}N2} - 1) \times 1{,}000$. In this study almost all the C and N isotope data were performed in duplicate, and the analytical reproducibility of the repeated sample measurements for the C and N isotope values conducted by the EA-IRMS was, respectively, better than ± 0.1% and ± 0.3%. The TOC abundance for the whole-rock samples, and the abundance of the TN_{bulk} for whole-rock samples and of N_{ker} for kerogen extracts were obtained from the peak areas of the major isotopes through the use of the calibrations for the $\delta^{13}C_{org}$, $\delta^{15}N_{bulk}$, and $\delta^{15}N_{ker}$ values, respectively. The analytical repeatability was better than ± 0.2 wt.% for the contents of TOC, TN_{bulk} and N_{ker}.

4. Results and Discussion

4.1. Evaluation of Primary Nitrogen Isotopic Signals

Continental run-off of OM from land plants may provide an additional source of N and may influence the isotope composition of marine sediments. In this study, the Dotternhausen sedimentary section from 1,050 to 980 cm is composed of organic-lean shales deposited prior to the T-CIE (Figure 2). These shale samples contain a considerable component of land plant-derived OM supported by low HI value (<400 mg HC/g TOC) and high oxygen index values (up to 100 mg CO_2/g TOC) (cf. Frimmel et al., 2004; Wang et al., 2020). In contrast, from 986 to 600 cm of this section, the OM in T-CIE fine-grained organic-rich sedimentary rocks (Figure 2) was primarily of marine origin (Frimmel et al., 2004; Wang et al., 2020) and thus likely reflect N biogeochemical processes in marine environments during the T-CIE.

The $\delta^{15}N$ of sedimentary rocks is a robust proxy to record the primary biomass signal of living organisms if it is not substantially imprinted by allochthonous inorganic N, diagenesis, metamorphism or metasomatism (e.g., Ader et al., 2006; Stüeken et al., 2016). Nitrogen in the sedimentary rocks is primarily present in organic- and clay-bound forms (mainly as ammonium (NH_4^+)). The presence of a large fraction of inorganic N

Table 1
Carbon and Nitrogen Data for the Dotternhausen Samples

Depth [cm]	TOC (wt.%)	$\delta^{13}C_{org}$ (‰, VPDB)	TN_{bulk} (wt.%)	$(C/N)_{bulk}$ (mol/mol)	$\delta^{15}N_{bulk}$ (‰, Air-N_2)	$\delta^{13}C_{ker}$ (‰, VPDB)	TN_{ker} (wt.%)	$\delta^{15}N_{ker}$ (‰, Air-N_2)	$(C/N)_{ker}$ (mol/mol)	$\Delta^{15}N_{bulk-ker}$ (‰)
621	6.3	−27.7	0.21	35.7	2.3	−27.6	0.86	1.5	56.2	0.8
635	12.5	−27.6	0.28	52.2	2.1	−28.1	0.79	1.6	52.2	0.5
648	16.8	−27.6	0.43	45.7	2.8	−28.3	1.29	2.5	42.0	0.3
669.5	10.6	−28.5	0.33	37.5	2.5	−28.8	0.98	2.0	58.9	0.5
687	11.7	−28.2	0.32	42.5	2.1	−28.3	1.04	1.8	56.6	0.3
705	18.0	−28.4	0.37	57.0	2.1	−28.9	1.20	2.2	55.5	−0.1
729	18.5	−29.2	0.33	65.9	4.0	−29.8	1.31	1.9	46.9	2.1
743	16.1	−30.6	0.14	52.2	2.0	−31.0	1.15	2.2	51.9	−0.2
760	21.9	−31.0	0.41	62.0	2.0	−31.6	1.32	2.0	52.0	−0.1
770	27.0	−32.0	0.53	59.7	2.2	−32.4	1.34	2.4	51.0	−0.2
775	17.7	−30.0	0.39	53.1	1.9	−29.7	1.29	1.2	54.4	0.7
782	10.9	−32.3	0.31	40.4	2.2	−32.6	1.07	2.0	49.4	0.2
785	16.4	−30.5	0.39	48.5	1.9	−30.7	1.25	1.1	51.1	0.9
790	22.8	−30.8	0.43	61.5	1.7	−31.4	1.13	0.3	53.6	1.5
792	14.8	−31.0	0.32	53.4	1.6	−31.7	0.52	1.1	53.6	0.5
817	19.1	−31.9	0.37	60.8	3.3	−32.4	1.09	1.4	52.2	1.9
819.5	19.1	−31.9	0.35	63.7	3.1	−32.2	1.26	1.3	52.1	1.7
822	20.9	−32.3	0.28	85.6	3.1	−32.6	1.27	1.6	56.1	1.5
825	17.9	−32.0	0.24	85.3	5.7	−32.7	1.13	1.6	49.1	4.1
836	12.2	−33.1	0.31	46.1	4.7	−33.4	1.04	2.0	50.6	2.7
859	17.2	−32.7	0.23	86.9	2.1	−33.3	1.13	2.1	51.3	0.0
871	15.4	−32.0	0.27	66.2	1.2	−32.4	1.18	2.0	50.7	−0.8
898	13.2	−32.1	0.39	39.4	1.0	−32.5	0.90	2.0	47.8	−1.0
919	16.4	−32.0	0.34	56.0	1.1	−32.5	1.13	1.9	48.7	−0.7
940	7.0	−32.2	0.15	53.4	0.9	−32.7	0.43	2.2	49.7	−1.4
964	12.4	−31.6	0.29	49.5	1.5	−32.2	1.02	2.2	52.2	−0.7
986	8.7	−29.2	0.20	50.7	0.8	−29.6	0.64	1.7	47.2	−0.8
1,003	0.8	−27.4	0.06	14.6	2.2	−27.5	0.35	2.0	53.4	0.2
1,020	0.6	−26.9	0.08	8.9	1.9	−27.0	0.29	1.6	48.8	0.2
1,030	0.6	−27.5	0.08	8.6	2.4	−27.4	0.28	1.6	50.0	0.8
1,040	0.6	−27.2	0.08	8.9	1.9	−26.4	0.28	1.6	53.4	0.3

(NH_4^+) can significantly affect organic-bound $\delta^{15}N$ values, especially in organic-lean sediments (e.g., Schubert & Calvert, 2001). Here, the high TOC content (15.6 wt.% on average) for the studied Dotternhausen T-CIE samples (Table 1) imply the negligible alteration on the primary $\delta^{15}N$ by inorganic N. The positive correlation between TOC and TN_{bulk} ($R^2 = 0.43$; $p = 0.00$; Figure 3a) observed for the studied T-CIE samples implies that most N was derived from marine organic matter. Furthermore, the lack of correlation between TN_{bulk} and detrital indicator aluminum (Al) concentration (Figure 3b) indicates the N contribution from detrital input does not compromise the robustness of the primary N isotope signal.

The release of NH_4^+ induced by OM remineralization in diagenetic settings can to some extent influence the whole rock $\delta^{15}N_{bulk}$ values. For instance, an obvious increase in $\delta^{15}N_{bulk}$ values by ~4‰ will be caused under oxic diagenetic conditions, whereas a minimal alteration on $\delta^{15}N_{bulk}$ values is often expected during anoxic

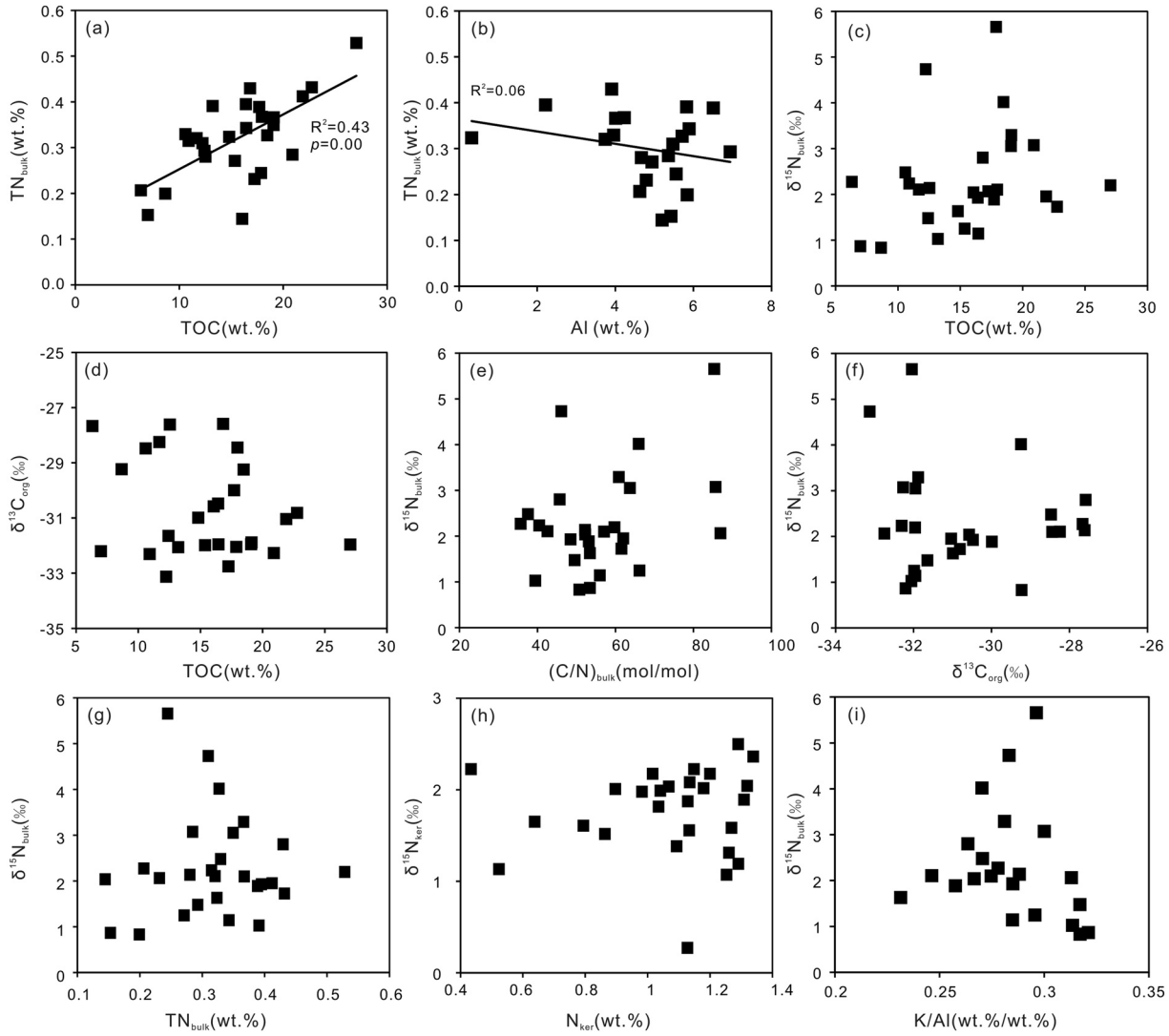

Figure 3. Cross-plots of geochemical data for the Dotternhausen Toarcian carbon isotope excursion samples. Data show: (a) Total nitrogen $(TN)_{bulk}$ versus total organic carbon (TOC), (b) TN_{bulk} versus Al, (c) $\delta^{15}N_{bulk}$ versus TOC, (d) $\delta^{13}C_{org}$ versus TOC, (e) $\delta^{15}N_{bulk}$ versus $(C/N)_{bulk}$, (f) $\delta^{15}N_{bulk}$ versus $\delta^{13}C_{org}$, (g) $\delta^{15}N_{bulk}$ versus TN_{bulk}, (h) $\delta^{15}N_{ker}$ versus N_{ker}, and (i) $\delta^{15}N_{bulk}$ versus K/Al. The data of Al and K concentrations are from Wang et al. (2020).

diagenesis that is accompanied by an isotopic fractionation of <1‰ (Ader et al., 2006; Altabet et al., 1999; Stüeken et al., 2016). In this study, early diagenetic influence on the studied $\delta^{15}N_{bulk}$ values can be discounted because fine-grained Dotternhausen sedimentary rocks across the T-CIE interval are enriched in TOC, prone to anoxic diagenesis, and were deposited in a strongly redox-stratified basin with oxic surface and euxinic bottom water masses (Röhl et al., 2001; Schwark & Frimmel, 2004; Wang et al., 2020) which further prevented oxic diagenesis. This inference is supported by the absence of negative correlations of $\delta^{15}N_{bulk}$ versus TOC and $\delta^{13}C_{org}$ versus TOC (Figures 3c,and 3d) that are often expected following early diagenetic alteration processes (e.g., Wang et al., 2018).

Thermal devolatilization of OM due to burial diagenesis and metamorphism tends to preferential free organic-bound ^{14}N, leading to a $\delta^{15}N_{bulk}$ increase by 1‰–2‰ for greenschist facies, 3‰–4‰ for lower amphibolite facies, and up to 6‰–12‰ for upper amphibolite facies (e.g., Ader et al., 2006). However, it is constrained that the OM of the Dotternhausen T-CIE samples was well preserved and did not apparently experience thermal volatilization (Wang et al., 2020), which suggests a negligible rise in the studied $\delta^{15}N_{bulk}$ values. On the other hand, the preferential release of ^{14}N due to thermal volatilization is typically accompanied by positive covariations of $\delta^{15}N_{bulk}$ versus $(C/N)_{bulk}$ and $\delta^{15}N_{bulk}$ versus $\delta^{13}C_{org}$, and negative

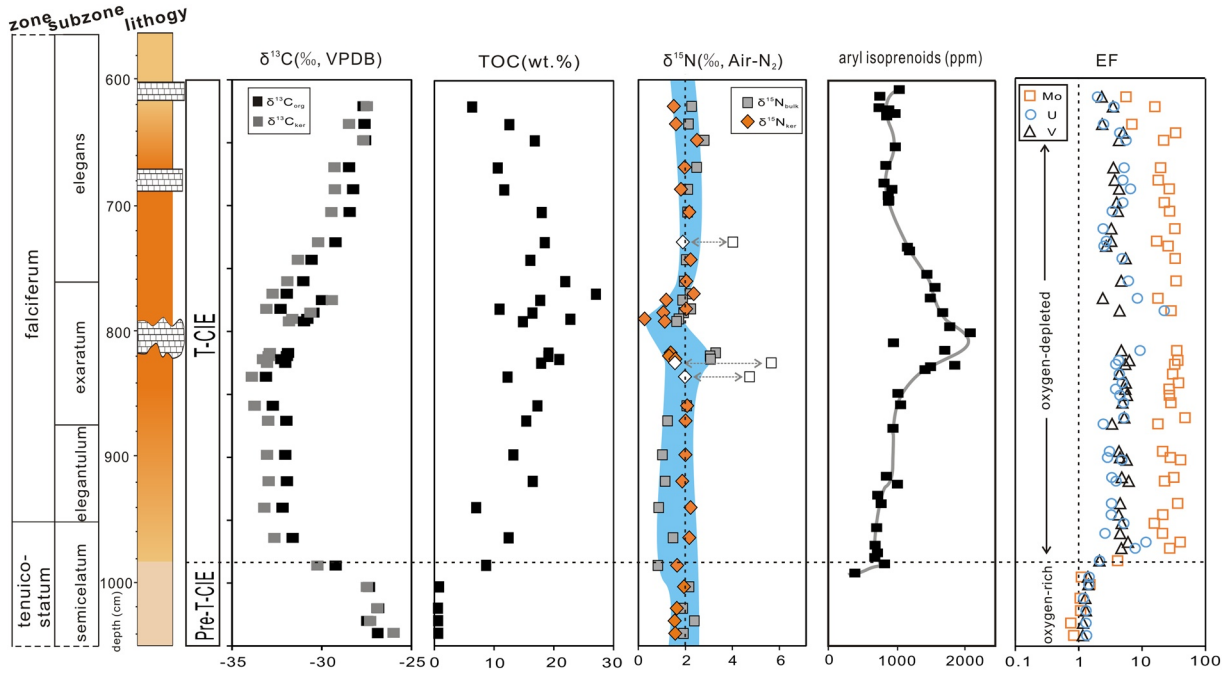

Figure 4. Chemostratigraphic $\delta^{13}C$, total organic carbon (TOC) content, $\delta^{15}N$, aryl isoprenoid content and enrichment factors (EFs) of Mo, V and U for Dotternhausen sedimentary section. Reliable N isotope values for the Dotternhausen samples are denoted in the $\delta^{15}N$ panel using a blue shading. The white diamonds and squares in the $\delta^{15}N$ panel denote the excluded samples that have large offsets between $\delta^{15}N_{bulk}$ and $\delta^{15}N_{ker}$ (see 4.1 for detailed discussion). The data of aryl isoprenoid content are from Schwark and Frimmel (2004). The Mo, V, U and aluminum (Al) data are from Wang et al. (2020). EF is calculated relative to upper continental crust (UCC; McLennan, 2001) using the equation of $[(element/Al)_{sample}/(element/Al)_{UCC}]$.

covariations of $\delta^{15}N_{bulk}$ versus TN_{bulk} and $\delta^{15}N_{ker}$ versus N_{ker} (Ader et al., 2006, 2016; Kipp et al., 2018; Mettam et al., 2019). The scarcity of such covariations (Figures 3e–3h) again implies the negligible systematic burial diagenetic or metamorphic alteration on the primarily deposited N isotope compositions of the Dotternhausen T-CIE samples. Furthermore, metasomatism can potentially substitute the organic-bound NH_4^+ by externally fluid-sourced potassium ions (K^+), due to equal charge and similar sizes, and change the primary $\delta^{15}N_{bulk}$ values (Ader et al., 2016; Stüeken et al., 2016). However, the lack of a relationship between $\delta^{15}N_{bulk}$ and K/Al (Figure 3i) rules out this possibility.

In addition, $\delta^{15}N_{ker}$ can be used to calibrate and evaluate the preservation extent of the primarily deposited N isotope signal imparted by the originally sinking biomass (e.g., Ader et al., 2016; Kipp et al., 2018; Stüeken et al., 2016, 2017). A majority of the studied samples show an overall minimal offset between $\delta^{15}N_{bulk}$ and $\delta^{15}N_{ker}$ ($\Delta^{15}N_{bulk-ker} = \delta^{15}N_{bulk}-\delta^{15}N_{ker}$, 0.2 ± 0.8‰; average ± 1 standard deviation), excluding three samples (DH-836, DH-825 and DH-729) with high $\delta^{15}N_{bulk}$ values (up to +5.7‰), where the offset is up to +4.1‰ (Figure 4; Table 1). The primary N isotope compositions of these three samples were likely affected by locally small-scale post-depositional modifications (Ader et al., 2016; Kipp et al., 2018; Stüeken et al., 2017) and will thus be excluded for further discussion. By contrast, the minimal $\delta^{15}N_{bulk}$-$\delta^{15}N_{ker}$ offset displayed for the rest of the Dotternhausen samples implies that the primary N isotopic signals are well preserved.

4.2. Marine N Biogeochemical Cycling During the Dotternhausen Toarcian Carbon Isotope Excursion

Well preserved primary N isotope compositions of sedimentary OM can serve as an effective proxy to reconstruct the input (e.g., diazotrophy which is an atmospheric N_2 fixation metabolism utilizing metal-based nitrogenase enzymes) and output (e.g., denitrification and/or anammox) fluxes of bioavailable N in marine environments. Diazotrophy relying on molybdenum (Mo)-based nitrogenase is the most representative form of N_2 fixation in natural environments (Stüeken et al., 2016; Tyrrell, 1999). In marine settings with aqueous Mo limitation, N_2 fixation can alternatively use vanadium (V)- or iron (Fe)-based nitrogenase.

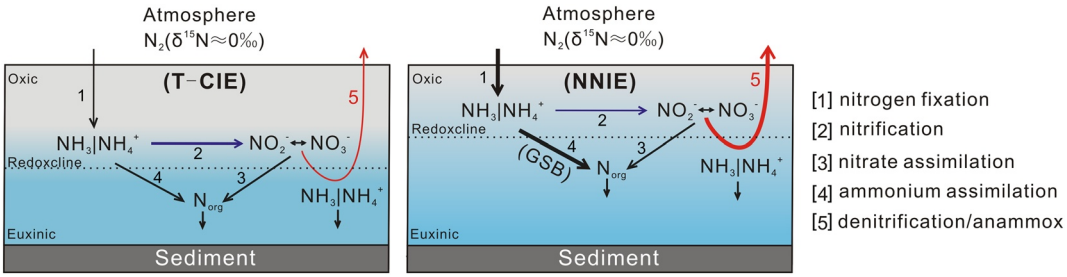

Figure 5. Schematic sketch showing N biogeochemical cycling in the Dotternhausen depositional setting across the Toarcian carbon isotope excursion (T-CIE) interval. During the maximum anoxia at the height of T-CIE (NNIE), thicker black arrows in [1] and [4] indicate enhanced nitrogen fixation and ammonium assimilation, respectively, while thicker red arrow in [5] denotes quantitative denitrification and/or anammox. NNIE: negative nitrogen isotope excursion (see Figure 4). GSB: green sulfur bacteria.

Culture experiments revealed that the expression of Mo- versus alternative-nitrogenase can be discerned by the N isotope values of the produced biomass (Bauersachs et al., 2009; Zhang et al., 2014). In these experiments, Mo-based diazotrophy had biomass $\delta^{15}N$ values between −4‰ and + 2‰, while alternative nitrogenase yields values as low as −7‰. In the modern ocean, aerobic N cycle is dominated by largely quantitative nitrification and partial denitrification and/or anammox in oxygen minimum zones (OMZs). This process leaves the remaining deep ocean NO_3^- pool higher $\delta^{15}N$ values with an average of ~ + 5‰ (e.g., Sigman & Fripiat, 2019; Tesdal et al., 2013). Biomass preserves this signature in marine sediments. Thus, in ancient sedimentary rocks, $\delta^{15}N$ values between −4‰ and + 2‰ can be confined to the dominant operation of Mo-based diazotrophy, while higher $\delta^{15}N$ values (> + 3‰) evidence water-column partial denitrification and/or anammox (e.g., Garvin et al., 2009; Gilleaudeau et al., 2020; Stüeken et al., 2016).

In the Dotternhausen sedimentary section, the initiation of the T-CIE corresponds to the onset of the prominent enrichment of Mo, V and uranium (U) which are redox-sensitive elements (Figure 4). These elements are more soluble and less particle-reactive under oxygen-rich seawater states, which tends not to express authigenic enrichment in the oxic sediments; on the other hand, these elements are less soluble and more particle-reactive under oxygen-depleted seawater conditions, which can lead to pronounced authigenic accumulation in sediments (Algeo & Maynard, 2004; Tribovillard et al., 2006). The obvious authigenic enrichment of the Mo, V and U in this study thus implies the development of bottom-water euxinic conditions during the deposition of the T-CIE Dotternhausen section. Furthermore, there is a strong correlation between the height of the T-CIE curve and aryl isoprenoid, green sulfur bacteria (GSB) biomarker abundance (see Figure 4; Wang et al., 2020) indicating that the peak of the T-CIE coincides with the highest level of euxinic conditions in the water column. Evidence for this anoxia was traditionally described to reflect the Toarcian OAE (e.g., Pearce et al., 2008; Thibault et al., 2018).

Both $\delta^{13}C$ for TOC and separated kerogen show similar negative excursion, reaching minimum values of −33.1‰ and −33.4‰, respectively (Figure 4; Table 1). The $\delta^{15}N$ values predominantly range between +0.3 and + 2.5‰ (average ± 1 standard deviation; $\delta^{15}N_{bulk}$ = +2.0 ± 0.6‰ and $\delta^{15}N_{ker}$ = +1.8 ± 0.5‰) (Figure 4; Table 1). Across the T-CIE, the increasing bottom-water euxinia facilitated the emergence of water-column denitrification and/or anammox at the redoxcline (Figure 5). However, the reliable $\delta^{15}N$ values between +0.3 and + 2.5‰ found in the uppermost *tenuicostatum* and lower *falciferum* zones (Figure 4) do not reflect the isotope effect of water-column partial denitrification and/or anammox (traditionally > + 3‰; cf. Garvin et al., 2009; Gilleaudeau et al., 2020; Stüeken et al., 2016). By contrast, such a N isotope signal is in accordance with Mo-based diazotrophy likely under N-limited conditions. The severe scarcity of bioavailable N in the coeval depositional environment was driven by quantitative denitrification and/or anammox which was accompanied by the lack of an isotopic effect. The other possibility is that the concentration of dissolved N may have been high in anoxic bottom waters similar to the situation in the modern Black Sea (Ader et al., 2016; Fulton et al., 2012; Stüeken et al., 2016). However, the lack of N exchange between bottom and surface waters may have limited the availability of this dissolved deep N pool to organisms in surface waters and likely caused N scarcity. Cyanobacteria may thus have enhanced the rate of N_2 fixation to compensate this bioavailable N famine, here marked by the lack of any large isotopic variability. A small

$\delta^{15}N$ depletion to ~0‰ is found in the middle of the *exaratum* subzone (Figure 4). This depletion correlates with the highest level of bottom-water euxinia (Schwark & Frimmel, 2004; Wang et al., 2020) and may be associated with enhanced Mo-based diazotrophic activity through which more atmospheric N_2 would have been fixed (~0‰) (Figure 5). Alternatively, this small negative $\delta^{15}N$ excursion is also coincident with highest abundance of aryl isoprenoid biomarkers, leading to elevated contribution of ^{14}N-enriched GSB biomass (Fogel & Cifuentes, 1993; Schwark & Frimmel, 2004) (Figures 4 and 5). Nonetheless, N famine occurred in surface waters as a result of N loss to the atmosphere (quantitative denitrification and/or anammox) and/or lack of mixing between bottom and surface waters during the deposition of the Dotternhausen T-CIE interval. In view of this, atmospheric N_2 was substantially fixed through Mo-based diazotrophs in order to keep pace with this seawater N scarcity.

4.3. Can the Northern European Epicontinental Shelf Settings Help to Validate an Evolved Oceanic Anoxic Event During the Toarcian Carbon Isotope Excursion?

T-CIE sedimentary profiles in the northern European epicontinental shelf are commonly marked by high abundance in TOC (e.g., Jenkyns, 2010). In addition to hydrographically restricted conditions (e.g., modern Black Sea), organic-rich sediments are also distributed in modern upwelling (unrestricted)-induced OMZ settings where partial denitrification and/or anammox is at play (Lam & Kuypers, 2011). By contrast, the studied T-CIE fine-grained organic-rich sedimentary rocks were deposited in a characteristic marine environment with enhanced water-column quantitative denitrification and/or anammox (see above). This finding convincingly manifests that the Dotternhausen fine-grained organic-rich rock deposition happened in a hydrographically restricted regime with minimal exchanges between bottom and surface waters during the T-CIE. Such hydrographic water-mass restriction heavily impeded bioavailable N replenishment from the bottom waters or open ocean and only accommodated an extremely limited NO_3^- inventory in surface waters. The restricted amount of NO_3^- was quantitatively consumed when the seawater became extensively euxinic during the T-CIE (Schwark & Frimmel, 2004). The reduced species of NH_4^+ acquired through enhanced N_2 fixation therewith succeeded NO_3^- as the dominant biologically available N form. Typically, under NH_4^+-replete conditions, biotic assimilation imparts a large isotope fractionation (−27‰ – −4‰) depending on the NH_4^+ abundance, followed by the formation of low $\delta^{15}N$ values of biomass (e.g., Higgins et al., 2012; Stüeken et al., 2016). However, this possibility is markedly inconsistent with the T-CIE $\delta^{15}N$ values (+0.3‰ – +2.5‰) of the Dotternhausen section (Figure 4). It further indicates that the ecosystem assimilating this newly fixed N was too small to outbalance the $\delta^{15}N$ values of the preserved biomass as a consequence of a restricted setting. An analog exhibiting such a restricted marine environment is the Black Sea across the Holocene during which the prominently prevalent biological N_2 fixation was accompanied by biomass $\delta^{15}N$ values of ~0‰ – +2‰ stimulated by the deficit in bioavailable N (Fulton et al., 2012; Tyrrell, 1999) owing to (near-) complete consumption of NO_3^-. This scenario has also been proposed for ancient Archean and mid-Proterozoic marine environments (Ossa Ossa et al., 2019; Stüeken et al., 2016).

Additionally, whole rock $\delta^{15}N$ data compiled from multiple shallow shelf T-CIE sedimentary successions including Rietheim (Switzerland), Réka Valley (Hungary), Yorkshire (UK), Winterborne Kingston (UK) and Mochras (UK) in the northern European epicontinental shelf range between −4‰ and +2‰ (Figure 6). However, the pelagic T-CIE profile from Dogna in Italy exhibits a slightly larger variation in $\delta^{15}N_{bulk}$ values between −3‰ and +4‰ (Figure 6). Environmental redox conditions during the deposition of the pelagic T-CIE Dogna sedimentary succession were proposed to have been unstable (Dickson et al., 2017). Nevertheless, $\delta^{15}N$ values up to +4‰ observed in this profile may also be tied to NO_3^- assimilation or partial denitrification and/or anammox in OMZs elsewhere in a likely oxygenated Tethyan Sea (see review from Ader et al., 2016). It is thus worth noting that the $\delta^{15}N$ records of other T-CIE profiles located in the shallow shelf settings fall in the Mo-based diazotrophic range. This N_2 fixation isotope record contradicts the possibility of existing water-column partial denitrification and/or anammox of marginal marine basins connected to the open ocean ($\delta^{15}N$ values traditionally > +3‰; e.g., Ader et al., 2016; Garvin et al., 2009; Gilleaudeau et al., 2020; Stüeken et al., 2016), but is in line with redox-controlled N biogeochemical cycle in hydrographically restricted environments.

To confirm the scenario for restricted marine settings, organic-rich sediment Mo/TOC mass ratio was used to constrain the degree of hydrographically restricted water-mass conditions of T-CIE sections deposited

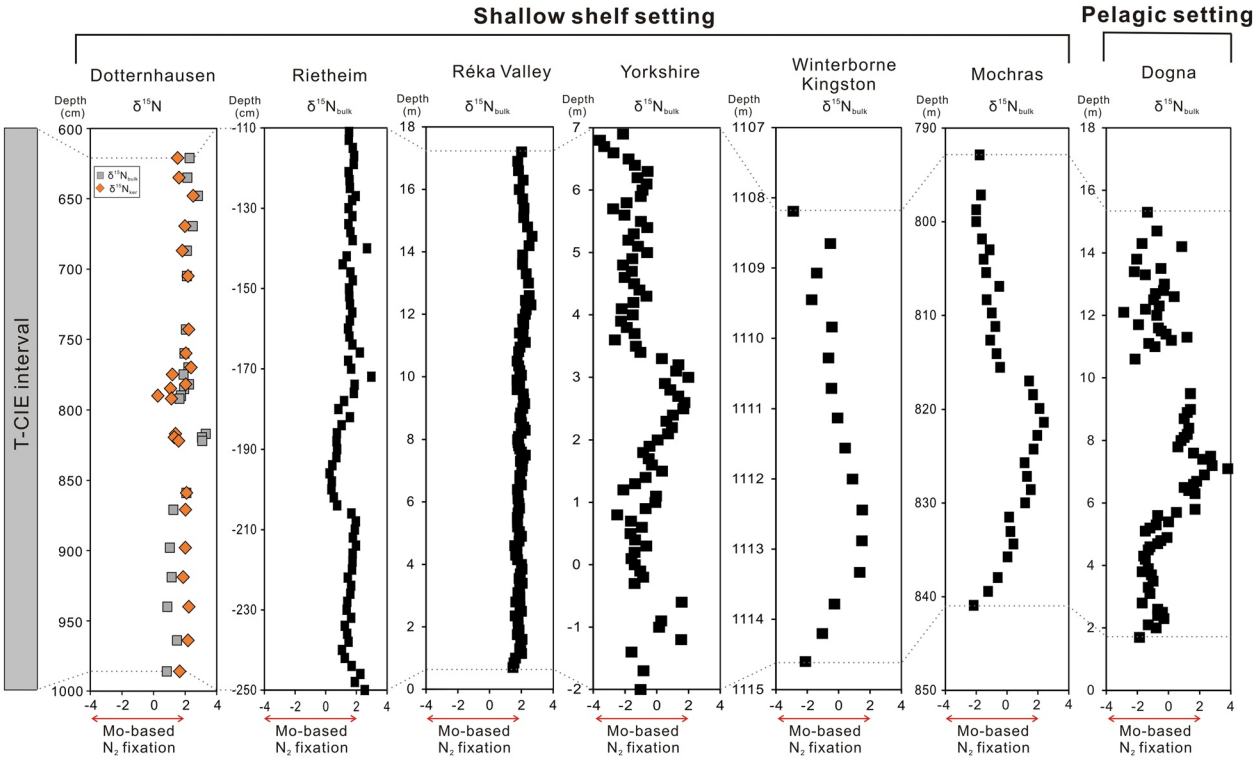

Figure 6. Comparison of $\delta^{15}N$ records among multiple Toarcian carbon isotope excursion sections. The $\delta^{15}N_{bulk}$ data of Rietheim (Switzerland) and Réka Valley (Hungary) sections are from Montero-Serrano et al. (2015) and Ruebsam et al. (2018), respectively. The $\delta^{15}N_{bulk}$ data of Yorkshire (represented by Hawsker Bottom; UK), Winterborne Kingston (UK), Mochras (UK) and Dogna (Italy) sections are from Jenkyns et al. (2001).

in the northern European epicontinental shelf. This proxy relies on the observation that the slope of the Mo versus TOC regression line is low at ~4.5 $\mu g \cdot g^{-1} \cdot wt.\%^{-1}$ (Figure 7a) in modern Black Sea organic-rich sediments deposited under severe hydrographic restriction with limited water-mass renewal (Algeo & Lyons, 2006). The occurrence of such a low Mo versus TOC regression line slope is due to basin-scale aqueous

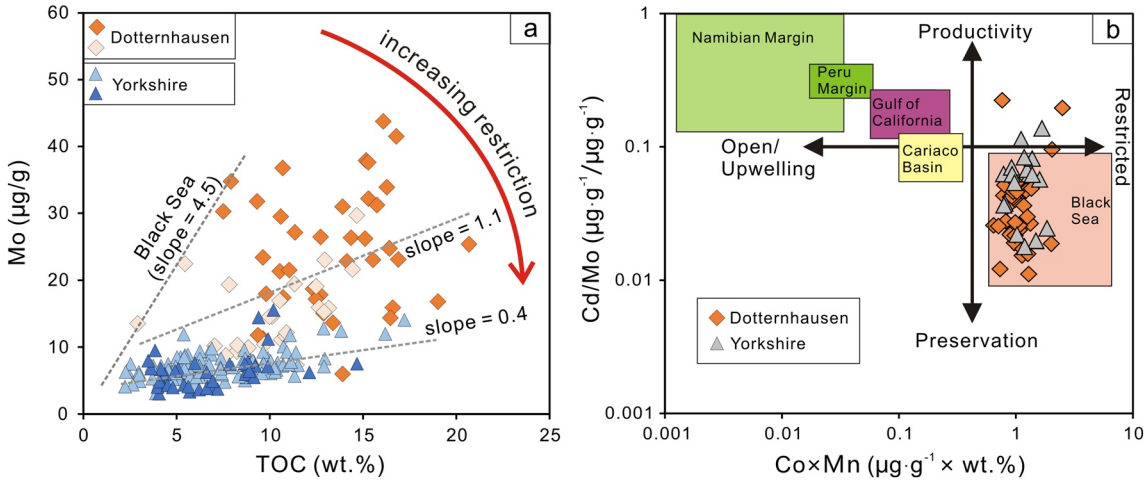

Figure 7. Cross-plots of Molybdenum (Mo) versus total organic carbon contents (a) and cadmium (Cd)/Mo versus cobalt (Co) × manganese (Mn) (b) for Dotternhausen and Yorkshire Toarcian carbon isotype excursion organic-rich samples. (a) The lower the slope the more depleted is the aqueous Mo reservoir due to hydrographically restricted water-mass circulation in coeval depositional settings (Algeo & Lyons, 2006). (b) the values of Cd/Mo and Co × Mn for modern organic-rich sediments from distinct depositional settings follow Sweere et al. (2016). Heavy and light blue triangles in a denoting the Yorkshire sample data are from Pearce et al. (2008) and Thibault et al. (2018), respectively. Gray triangles in b denoting the Yorkshire sample data are from McArthur (2019). Heavy orange diamonds in a and b, and light ones in a denoting Dotternhausen sample data are from Wang et al. (2020) and Dickson et al. (2017), respectively.

Mo drawdown to the sediment along with limited resupply. When hydrographic restriction condition decreased, the increase in open ocean water mass renewal and Mo replenishment led to high slope values in organic-rich marine sediments. Slopes in Mo versus TOC space for T-CIE sedimentary successions are very variable with values between 0.4 and 1.1 $\mu g \cdot g^{-1} \cdot wt.\%^{-1}$, implying that for example the depositional environment of the Yorkshire succession was more restricted than that of Dotternhausen (Figure 7a). Furthermore, both slope values are lower than ~4.5 $\mu g \cdot g^{-1} \cdot wt.\%^{-1}$ (Figure 7a), supporting that their depositional settings were even more restricted than the modern Black Sea (Figure 7a). Given the drawdown of dissolved Mo is very fast when adequate amounts of aqueous hydrogen sulphide are present (Algeo & Maynard, 2004; Reinhard et al., 2013), the persistently high Mo enrichment throughout the entire Dotternhausen T-CIE section (Figure 4) points to limited but permanent Mo feeding from a larger oxic Mo reservoir that is, open ocean (Algeo & Lyons, 2006). The lack of evidence for quantitative Mo drawdown in pelagic Tethyan black shales of the Dogna sedimentary succession indicates that Mo likely remained dissolved in coeval oxic seawaters while their light δ^{98}Mo values (Dickson et al., 2017) further support that the water column, at least at the site of deposition, was not anoxic and sulfidic (euxinic) during the T-CIE. This may explain why the Dogna sedimentary succession did not record the N isotopic effect of water-column denitrification and/or anammox at the site of the deposition—though the water-column of deposition was neither euxinic nor sulfidic oxygen-depleted OMZ.

In addition, hydrographic conditions can also be evaluated using a cross-plot of sedimentary cadmium (Cd)/Mo versus manganese×cobalt (Mn*Co) since distinct hydrographic regimes can be effectively constrained by modern high-TOC marine sediment Cd/Mo and Co×Mn values (Figure 7b; cf. Sweere et al., 2016, 2020). High Cd uptake in organic material relative to Mo often promotes high Cd/Mo ratios (>0.1) in organic-rich sediments in upwelling (unrestricted) regions of the modern ocean (Conway & John, 2015). In restricted settings, oxygen deficit is in favor of Cd and Mo deposition but relatively weak marine productivity limits organic-driven output channel of Cd, resulting in low sedimentary Cd/Mo ratios (<0.1). The contents of Co and Mn in rivers and/or surface seawaters are significantly enriched compared to open-ocean sub-surface waters which feed upwelling systems, and thus the supply of both elements is typically higher in restricted basins (Sweere et al., 2016 and references therein). The different behaviors of these elements eventually promote high Co×Mn values (>0.4 $\mu g \cdot g^{-1} \times$ wt.%) in organic-rich sediments that are deposited under restricted settings, whereas low Co×Mn values (<0.4 $\mu g \cdot g^{-1} \times$ wt.%) in the counterpart from upwelling (unrestricted) settings. An empirical comparison between elemental data from the representative T-CIE sedimentary successions with the modern marine sediment records is further indicative of hydrographically restricted water-mass conditions for the northern European epicontinental shelf seas (Figure 7b).

Collectively, combined N isotope and elemental concentration data of sedimentary successions deposited during the T-CIE add an important insight in the evolution of the ocean redox structure during the early Jurassic. These data support that the deoxygenated marine conditions commonly identified in several T-CIE localities from the northern European epicontinental shelf do not reflect the redox structure of the coeval Tethyan ocean, but rather indicate the development of oxygen-deficient basins. However, testing whether the global deep-ocean anoxia existed during the T-CIE requires robust redox evaluation (e.g., by trace element geochemistry and Fe speciation) of deep open ocean sedimentary successions.

5. Conclusion

Combined $\delta^{15}N_{bulk}$ and $\delta^{15}N_{ker}$ data obtained from the well-recognized T-CIE sedimentary section of Dotternhausen, SW Germany, are used to investigate the N biogeochemical cycle and its isotopic effect during the Early Toarcian marine deoxygenation. The $\delta^{15}N_{bulk}$ and $\delta^{15}N_{ker}$ values range predominantly between +0.3‰ and +2.5‰, implying enhanced N_2 fixation by cyanobacteria using Mo-based nitrogenase enzyme to keep pace with bioavailable N loss as a result of quantitative denitrification and/or anammox in a strongly redox-stratified marine environment lacking exchanges between bottom and surface water masses. This inference is further confirmed by the sedimentary N isotope records ranging between −4‰ and +2‰ from other northern European epicontinental shallow-shelf sections. The N_2-fixing signal exhibited in these T-CIE sections contradicts the typical sedimentary $\delta^{15}N$ values (>3‰) induced by partial water-column denitrification and/or anammox in marginal marine settings well connected to the open ocean. Instead, this study proposes the development of oxygen-deficient basins on the northern European epicontinental shelf.

In such hydrographically restricted marine environments, dissolved N pool suffered extensive denitrification and/or anammox which led to severe bioavailable N scarcity and thus stimulated Mo-based diazotrophic activity. These oxygen-depleted restricted settings situated on the northern European epicontinental shelf cannot thus be considered for evaluating the redox landscape of the coeval open ocean during the T-CIE. A robust redox evaluation of sedimentary successions deposited in both Tethyan and Panthalassan oceans is thus still missing for validating the putative global deep ocean anoxia across the T-CIE interval.

Data Availability Statement

Geochemical data for this research are available in the Zenodo repository at https://zenodo.org/record/4778565#.YKe1LqgzaUl.

Acknowledgments
We would like to thank LafargeHolcim GmbH Dotternhausen for providing drill core material and its Head of the Fossil Museum Dr. Annette Schmid-Röhl for scientific discussion. Yunfeng Wang would like to thank the China Scholarship Council (201706400079) for the financial support. Frantz Ossa Ossa and Ronny Schoenberg acknowledge financial support by the German Research Foundation (DFG) project SCHO1071/11-1. We are greatly indebted to Eva Stüeken and the two anonymous reviewers for their constructive comments that greatly helped to improve the quality of the manuscript. Open access funding enabled and organized by Projekt DEAL.

References

Ader, M., Cartigny, P., Boudou, J. P., Oh, J. H., Petit, E., & Javoy, M. (2006). Nitrogen isotopic evolution of carbonaceous matter during metamorphism: Methodology and preliminary results. *Chemical Geology*, *232*(3–4), 152–169. https://doi.org/10.1016/j.chemgeo.2006.02.019

Ader, M., Thomazo, C., Sansjofre, P., Busigny, V., Papineau, D., Laffont, R., et al. (2016). Interpretation of the nitrogen isotopic composition of Precambrian sedimentary rocks: Assumptions and perspectives. *Chemical Geology*, *429*, 93–110. https://doi.org/10.1016/j.chemgeo.2016.02.010

Algeo, T. J., & Lyons, T. W. (2006). Mo–total organic carbon covariation in modern anoxic marine environments: Implications for analysis of paleoredox and paleohydrographic conditions. *Paleoceanography*, *21*, PA1016. https://doi.org/10.1029/2004pa001112

Algeo, T. J., & Maynard, J. B. (2004). Trace-element behavior and redox facies in core shales of Upper Pennsylvanian Kansas-type cyclothems. *Chemical Geology*, *206*(3–4), 289–318. https://doi.org/10.1016/j.chemgeo.2003.12.009

Altabet, M. A., Pilskaln, C., Thunell, R., Pride, C., Sigman, D., Chavez, F., & Francois, R. (1999). The nitrogen isotope biogeochemistry of sinking particles from the margin of the Eastern North Pacific. *Deep Sea Research Part I: Oceanographic Research Papers*, *46*(4), 655–679. https://doi.org/10.1016/s0967-0637(98)00084-3

Baudin, F., Herbin, J.-P., & Vandenbroucke, M. (1990). Mapping and geochemical characterization of the Toarcian organic matter in the Mediterranean Tethys and Middle East. *Organic Geochemistry*, *16*(4–6), 677–687. https://doi.org/10.1016/0146-6380(90)90109-d

Bauersachs, T., Schouten, S., Compaoré, J., Wollenzien, U., Stal, L. J., & Sinninghe Damsteé, J. S. (2009). Nitrogen isotopic fractionation associated with growth on dinitrogen gas and nitrate by cyanobacteria. *Limnology & Oceanography*, *54*(4), 1403–1411. https://doi.org/10.4319/lo.2009.54.4.1403

Bour, I., Mattioli, E., & Pittet, B. (2007). Nannofacies analysis as a tool to reconstruct paleoenvironmental changes during the Early Toarcian anoxic event. *Palaeogeography, Palaeoclimatology, Palaeoecology*, *249*(1–2), 58–79. https://doi.org/10.1016/j.palaeo.2007.01.013

Brazier, J. M., Suan, G., Tacail, T., Simon, L., Martin, J. E., Mattioli, E., & Balter, V. (2015). Calcium isotope evidence for dramatic increase of continental weathering during the Toarcian oceanic anoxic event (Early Jurassic). *Earth and Planetary Science Letters*, *411*, 164–176. https://doi.org/10.1016/j.epsl.2014.11.028

Chandler, M. A., Rind, D., & Ruedy, R. (1992). Pangaean climate during the Early Jurassic: GCM simulations and the sedimentary record of paleoclimate. *GSA Bulletin*, *104*(5), 543–559. https://doi.org/10.1130/0016-7606(1992)104<0543:pcdtej>2.3.co;2

Cohen, A. S., Coe, A. L., Harding, S. M., & Schwark, L. (2004). Osmium isotope evidence for the regulation of atmospheric CO_2 by continental weathering. *Geology*, *32*(2), 157–160. https://doi.org/10.1130/g20158.1

Conway, T. M., & John, S. G. (2015). The cycling of iron, zinc and cadmium in the North East Pacific Ocean–Insights from stable isotopes. *Geochimica et Cosmochimica Acta*, *164*, 262–283. https://doi.org/10.1016/j.gca.2015.05.023

Dera, G., Brigaud, B., Monna, F., Laffont, R., Pucéat, E., Deconinck, J. F., et al. (2011). Climatic ups and downs in a disturbed Jurassic world. *Geology*, *39*(3), 215–218. https://doi.org/10.1130/g31579.1

Dickson, A. J., Gill, B. C., Ruhl, M., Jenkyns, H. C., Porcelli, D., Idiz, E., et al. (2017). Molybdenum-isotope chemostratigraphy and paleoceanography of the Toarcian Oceanic Anoxic Event (Early Jurassic). *Paleoceanography*, *32*, 813–829. https://doi.org/10.1002/2016pa003048

Durand, B., & Nicaise, G. (1980). Procedures for kerogen isolation. In B. Durand (Ed.), *Kerogen insoluble organic matter from sedimentary rocks*. 35–53: Editions Technip.

Fantasia, A., Föllmi, K. B., Adatte, T., Spangenberg, J. E., & Montero-Serrano, J.-C. (2018). The Early Toarcian oceanic anoxic event: Paleoenvironmental and paleoclimatic change across the Alpine Tethys (Switzerland). *Global and Planetary Change*, *162*, 53–68. https://doi.org/10.1016/j.gloplacha.2018.01.008

Fogel, M. L., & Cifuentes, L. A. (1993). Isotope Fractionation during Primary Production. In M. H. Engel, & S. A. Macko (Eds.), *Organic Geochemistry*. (73–98). Springer, Boston, MA. https://doi.org/10.1007/978-1-4615-2890-6_3

Frimmel, A., Oschmann, W., & Schwark, L. (2004). Chemostratigraphy of the Posidonia Black Shale, SW Germany: I. Influence of sea-level variation on organic facies evolution. *Chemical Geology*, *206*(3–4), 199–230. https://doi.org/10.1016/j.chemgeo.2003.12.007

Fulton, J. M., Arthur, M. A., & Freeman, K. H. (2012). Black Sea nitrogen cycling and the preservation of phytoplankton $\delta^{15}N$ signals during the Holocene. *Global Biogeochemical Cycles*, *26*, GB2030. https://doi.org/10.1029/2011GB004196

Garvin, J., Buick, R., Anbar, A. D., Arnold, G. L., & Kaufman, A. J. (2009). Isotopic evidence for an aerobic nitrogen cycle in the latest Archean. *Science*, *323*(5917), 1045–1048. https://doi.org/10.1126/science.1165675

Gilleaudeau, G. J., Sahoo, S. K., Ostrander, C. M., Owens, J. D., Poulton, S. W., Lyons, T. W., & Anbar, A. D. (2020). Molybdenum isotope and trace metal signals in an iron-rich Mesoproterozoic ocean: A snapshot from the Vindhyan Basin, India. *Precambrian Research*, *343*, 105718. https://doi.org/10.1016/j.precamres.2020.105718

Harries, P. J., & Little, C. T. S. (1999). The early Toarcian (Early Jurassic) and the Cenomanian–Turonian (Late Cretaceous) mass extinctions: Similarities and contrasts. *Palaeogeography, Palaeoclimatology, Palaeoecology*, *154*(1-2), 39–66. https://doi.org/10.1016/S0031-0182(99)00086-3

Hermoso, M., & Pellenard, P. (2014). Continental weathering and climatic changes inferred from clay mineralogy and paired carbon isotopes across the early to middle Toarcian in the Paris Basin. *Palaeogeography, Palaeoclimatology, Palaeoecology*, *399*, 385–393. https://doi.org/10.1016/j.palaeo.2014.02.007

Hesselbo, S. P., Gröcke, D. R., Jenkyns, H. C., Bjerrum, C. J., Farrimond, P., Bell, H. S. M., & Green, O. W. (2000). Massive dissociation of gas hydrate during a Jurassic oceanic anoxic event. *Nature*, *406*, 392–395. https://doi.org/10.1038/35019044

Hesselbo, S. P., Jenkyns, H. C., Duarte, L. V., & Oliveira, L. C. V. (2007). Carbon-isotope record of the Early Jurassic (Toarcian) Oceanic Anoxic Event from fossil wood and marine carbonate (Lusitanian Basin, Portugal). *Earth and Planetary Science Letters*, *253*(3–4), 455–470. https://doi.org/10.1016/j.epsl.2006.11.009

Higgins, M. B., Robinson, R. S., Husson, J. M., Carter, S. J., & Pearson, A. (2012). Dominant eukaryotic export production during ocean anoxic events reflects the importance of recycled NH_4^+. *Proceedings of the National Academy of Sciences*, *109*(7), 2269–2274. https://doi.org/10.1073/pnas.1104313109

Jenkyns, H. C. (1988). The early Toarcian (Jurassic) anoxic event; stratigraphic, sedimentary and geochemical evidence. *American Journal of Science*, *288*(2), 101–151. https://doi.org/10.2475/ajs.288.2.101

Jenkyns, H. C. (2010). Geochemistry of oceanic anoxic events. *Geochemistry, Geophysics, Geosystems*, *11*(3), Q03004. https://doi.org/10.1029/2009gc002788

Jenkyns, H. C., Gröcke, D. R., & Hesselbo, S. P. (2001). Nitrogen isotope evidence for water mass denitrification during the early Toarcian (Jurassic) oceanic anoxic event. *Paleoceanography*, *16*(6), 593–603. https://doi.org/10.1029/2000pa000558

Kemp, D. B., Coe, A. L., Cohen, A. S., & Schwark, L. (2005). Astronomical pacing of methane release in the Early Jurassic period. *Nature*, *437*, 396–399. https://doi.org/10.1038/nature04037

Kipp, M. A., Stüeken, E. E., Yun, M., Bekker, A., & Buick, R. (2018). Pervasive aerobic nitrogen cycling in the surface ocean across the Paleoproterozoic Era. *Earth and Planetary Science Letters*, *500*, 117–126. https://doi.org/10.1016/j.epsl.2018.08.007

Lam, P., & Kuypers, M. M. (2011). Microbial nitrogen cycling processes in oxygen minimum zones. *Annual review of marine science*, *3*, 317–345. https://doi.org/10.1146/annurev-marine-120709-142814

Little, C. T. S., & Benton, M. J. (1995). Early Jurassic mass extinction: A global long-term event. *Geology*, *23*(6), 495–498. https://doi.org/10.1130/0091-7613(1995)023<0495:ejmeag>2.3.co;2

McArthur, J. M. (2019). Early Toarcian black shales: A response to an oceanic anoxic event or anoxia in marginal basins? *Chemical Geology*, *522*, 71–83. https://doi.org/10.1016/j.chemgeo.2019.05.028

McArthur, J. M., Algeo, T. J., van de Schootbrugge, B., Li, Q., & Howarth, R. J. (2008). Basinal restriction, black shales, Re-Os dating, and the Early Toarcian (Jurassic) oceanic anoxic event. *Paleoceanography*, *23*(4), PA4217. https://doi.org/10.1029/2008pa001607

McElwain, J. C., Wade-Murphy, J., & Hesselbo, S. P. (2005). Changes in carbon dioxide during an oceanic anoxic event linked to intrusion into Gondwana coals. *Nature*, *435*(7041), 479–482. https://doi.org/10.1038/nature03618

McLennan, S. M. (2001). Relationships between the trace element composition of sedimentary rocks and upper continental crust. *Geochemistry, Geophysics, Geosystems*, *2*(4), 1021. https://doi.org/10.1029/2000GC000109

Mettam, C., Zerkle, A. L., Claire, M. W., Prave, A. R., Poulton, S. W., & Junium, C. K. (2019). Anaerobic nitrogen cycling on a Neoarchaean ocean margin. *Earth and Planetary Science Letters*, *527*, 115800. https://doi.org/10.1016/j.epsl.2019.115800

Montero-Serrano, J. C., Föllmi, K. B., Adatte, T., Spangenberg, J. E., Tribovillard, N., Fantasia, A., & Suan, G. (2015). Continental weathering and redox conditions during the early Toarcian Oceanic anoxic event in the northwestern Tethys: Insight from the Posidonia Shale section in the Swiss Jura Mountains. *Palaeogeography, Palaeoclimatology, Palaeoecology*, *429*, 83–99. https://doi.org/10.1016/j.palaeo.2015.03.043

Ossa Ossa, F., Hofmann, A., Spangenberg, J. E., Poulton, S. W., Stüeken, E. E., Schoenberg, R., et al. (2019). Limited oxygen production in the Mesoarchean ocean. *Proceedings of the National Academy of Sciences*, *116*(14), 6647–6652. https://doi.org/10.1073/pnas.1818762116

Pálfy, J., & Smith, P. L. (2000). Synchrony between Early Jurassic extinction, oceanic anoxic event, and the Karoo-Ferrar flood basalt volcanism. *Geology*, *28*(8), 747–750. https://doi.org/10.1130/0091-7613(2000)28<747:SBEJEO>2.0.CO;2

Pearce, C. R., Cohen, A. S., Coe, A. L., & Burton, K. W. (2008). Molybdenum isotope evidence for global ocean anoxia coupled with perturbations to the carbon cycle during the Early Jurassic. *Geology*, *36*(3), 231–234. https://doi.org/10.1130/g24446a.1

Reinhard, C. T., Planavsky, N. J., Robbins, L. J., Partin, C. A., Gill, B. C., Lalonde, S. V., et al. (2013). Proterozoic ocean redox and biogeochemical stasis. *Proceedings of the National Academy of Sciences*, *110*(14), 5357–5362. https://doi.org/10.1073/pnas.1208622110

Remírez, M. N., & Algeo, T. J. (2020). Paleosalinity determination in ancient epicontinental seas: A case study of the T-OAE in the Cleveland Basin (UK). *Earth-Science Reviews. 201*. https://doi.org/10.1016/j.earscirev.2019.103072

Röhl, H.-J., & Schmid-Röhl, A. (2005). Lower Toarcian (Upper Liassic) black shales of the Central European Epicontinental Basin: A sequence stratigraphic case study from the SW German Posidonia Shale. In N. B. Harris (Ed.), The Deposition of Organic-Carbon-Rich Sediments: Models, Mechanisms, and Consequences, 82, 165–189. Society for Sedimentary Geology Special Publication. https://doi.org/10.2110/pec.05.82.0165

Röhl, H.-J., Schmid-Röhl, A., Oschmann, W., Frimmel, A., & Schwark, L. (2001). The Posidonia Shale (Lower Toarcian) of SW-Germany: an oxygen-depleted ecosystem controlled by sea level and palaeoclimate. *Palaeogeography, Palaeoclimatology, Palaeoecology*, *165*(1–2), 27–52. https://doi.org/10.1016/s0031-0182(00)00152-8

Rosales, I., Barnolas, A., Goy, A., Sevillano, A., Armendáriz, M., & López-García, J. M. (2018). Isotope records (C-O-Sr) of late Pliensbachian-early Toarcian environmental perturbations in the westernmost Tethys (Majorca Island, Spain). *Palaeogeography, Palaeoclimatology, Palaeoecology*, *497*, 168–185. https://doi.org/10.1016/j.palaeo.2018.02.016

Ruebsam, W., Mayer, B., & Schwark, L. (2019). Cryosphere carbon dynamics control early Toarcian global warming and sea level evolution. *Global and Planetary Change*, *172*, 440–453. https://doi.org/10.1016/j.gloplacha.2018.11.003

Ruebsam, W., Müller, T., Kovács, J., Pálfy, J., & Schwark, L. (2018). Environmental response to the early Toarcian carbon cycle and climate perturbations in the northeastern part of the West Tethys shelf. *Gondwana Research*, *59*, 144–158. https://doi.org/10.1016/j.gr.2018.03.013

Ruebsam, W., Reolid, M., & Schwark, L. (2020). $\delta^{13}C$ of terrestrial vegetation records Toarcian CO_2 and climate gradients. *Scientific Reports*, *10*, 117. https://doi.org/10.1038/s41598-019-56710-6

Ruvalcaba Baroni, I., Pohl, A., van Helmond, N. A. G. M., Papadomanolaki, N. M., Coe, A. L., Cohen, A. S., et al. (2018). Ocean circulation in the Toarcian (Early Jurassic): A key control on deoxygenation and carbon burial on the European Shelf. *Paleoceanography and Paleoclimatology*, *33*(9), 994–1012. https://doi.org/10.1029/2018PA003394

Sælen, G., Tyson, R. V., Telnæs, N., & Talbot, M. R. (2000). Contrasting watermass conditions during deposition of the Whitby Mudstone (Lower Jurassic) and Kimmeridge clay (upper Jurassic) formations, UK. *Palaeogeography, Palaeoclimatology, Palaeoecology*, *163*(3–4), 163–196. https://doi.org/10.1016/S0031-0182(00)00150-4

Schubert, C. J., & Calvert, S. E. (2001). Nitrogen and carbon isotopic composition of marine and terrestrial organic matter in Arctic Ocean sediments: Implications for nutrient utilization and organic matter composition. *Deep Sea Research Part I: Oceanographic Research Papers*, *48*(3), 789–810. https://doi.org/10.1016/s0967-0637(00)00069-8

Schwark, L., & Frimmel, A. (2004). Chemostratigraphy of the Posidonia Black Shale, SW-Germany: II. Assessment of extent and persistence of photic-zone anoxia using aryl isoprenoid distributions. *Chemical Geology*, *206*(3–4), 231–248. https://doi.org/10.1016/j.chemgeo.2003.12.008

Sigman, D. M., & Fripiat, F. (2019). Nitrogen isotope in the ocean. In J. Kirk Cochran H. J. Bokuniewicz & P. L. Yager (Eds.), Encyclopedia of Ocean Sciences, 3rd ed.1, 263–278. https://doi.org/10.1016/B978-0-12-409548-9.11605-7

Song, J., Littke, R., & Weniger, P. (2017). Organic geochemistry of the lower Toarcian Posidonia Shale in NW Europe. *Organic Geochemistry*, *106*, 76–92. https://doi.org/10.1016/j.orggeochem.2016.10.014

Spangenberg, J. E., Bagnoud-Velásquez, M., Boggiani, P. C., & Gaucher, C. (2014). Redox variations and bioproductivity in the Ediacaran: Evidence from inorganic and organic geochemistry of the Corumbá Group, Brazil. *Gondwana Research*, *26*(3–4), 1186–1207. https://doi.org/10.1016/j.gr.2013.08.014

Spangenberg, J. E., & Frimmel, H. E. (2001). Basin-internal derivation of hydrocarbons in the Witwatersrand Basin, South Africa: Evidence from bulk and molecular $\delta^{13}C$ data. *Chemical Geology*, *173*(4), 339–355. https://doi.org/10.1016/s0009-2541(00)00283-7

Spangenberg, J. E., & Herlec, U. (2006). Hydrocarbon biomarkers in the Topla-Mežica zinc– lead deposits, Northern Karavanke/Drau Range, Slovenia: Paleoenvironment at the site of ore formation. *Economic Geology*, *101*(5), 997–1021. https://doi.org/10.2113/gsecongeo.101.5.997

Spangenberg, J. E., Jacomet, S., & Schibler, J. (2006). Chemical analyses of organic residues in archaeological pottery from Arbon Bleiche 3, Switzerland-evidence for dairying in the late Neolithic. *Journal of Archaeological Science*, *33*(1), 1–13. https://doi.org/10.1016/j.jas.2005.05.013

Spangenberg, J. E., & Macko, S. A. (1998). Organic geochemistry of the San Vicente Mississippi Valley-type zinc–lead district, eastern Pucará Basin, Peru. *Chemical Geology*, *146*(1–2), 1–23. https://doi.org/10.1016/s0009-2541(97)00158-7

Stüeken, E. E., Kipp, M. A., Koehler, M. C., & Buick, R. (2016). The evolution of Earth's biogeochemical nitrogen cycle. *Earth-Science Reviews*, *160*, 220–239. https://doi.org/10.1016/j.earscirev.2016.07.007

Stüeken, E. E., Zaloumis, J., Meixnerová, J., & Buick, R. (2017). Differential metamorphic effects on nitrogen isotopes in kerogen extracts and bulk rocks. *Geochimica et Cosmochimica Acta*, *217*, 80–94. https://doi.org/10.1016/j.gca.2017.08.019

Svensen, H., Planke, S., Chevallier, L., Malthe-Sørenssen, A., Corfu, F., & Jamtveit, B. (2007). Hydrothermal venting of greenhouse gases triggering Early Jurassic global warming. *Earth and Planetary Science Letters*, *256*(3–4), 554–566. https://doi.org/10.1016/j.epsl.2007.02.013

Sweere, T., van den Boorn, S., Dickson, A. J., & Reichart, G. J. (2016). Definition of new trace-metal proxies for the controls on organic matter enrichment in marine sediments based on Mn, Co, Mo and Cd concentrations. *Chemical Geology*, *441*, 235–245. https://doi.org/10.1016/j.chemgeo.2016.08.028

Sweere, T. C., Dickson, A. J., Jenkyns, H. C., Porcelli, D., & Henderson, G. M. (2020). Zinc- and cadmium-isotope evidence for redox-driven perturbations to global micronutrient cycles during Oceanic Anoxic Event 2 (Late Cretaceous). *Earth and Planetary Science Letters*, *546*, 116427. https://doi.org/10.1016/j.epsl.2020.116427

Tesdal, J.-E., Galbraith, E. D., & Kienast, M. (2013). Nitrogen isotopes in bulk marine sediment: Linking seafloor observations with subseafloor record. *Biogeosciences*, *10*, 101–118. https://doi.org/10.5194/bg-10-101-2013

Them, T. R., Gill, B. C., Selby, D., Gröcke, D. R., Friedman, R. M., & Owens, J. D. (2017). Evidence for rapid weathering response to climatic warming during the Toarcian Oceanic Anoxic Event. *Scientific Reports*, *7*, 5003. https://doi.org/10.1038/s41598-017-05307-y

Thibault, N., Ruhl, M., Ullmann, C. V., Korte, C., Kemp, D. B., Gröcke, D. R., & Hesselbo, S. P. (2018). The wider context of the lower Jurassic Toarcian oceanic anoxic event in Yorkshire coastal outcrops, UK. *Proceedings of the Geologists' Association*, *129*(3), 372–391. https://doi.org/10.1016/j.pgeola.2017.10.007

Tribovillard, N., Algeo, T. J., Lyons, T., & Riboulleau, A. (2006). Trace metals as paleoredox and paleoproductivity proxies: An update. *Chemical Geology*, *232*(1–2), 12–32. https://doi.org/10.1016/j.chemgeo.2006.02.012

Tyrrell, T. (1999). The relative influences of nitrogen and phosphorus on oceanic primary production. *Nature*, *400*(6744), 525–531. https://doi.org/10.1038/22941

van Acken, D., Tütken, T., Daly, J. S., Schmid-Röhl, A., & Orr, P. J. (2019). Rhenium-osmium geochronology of the Toarcian Posidonia Shale, SW Germany. *Palaeogeography, Palaeoclimatology, Palaeoecology*, *534*, 109294. https://doi.org/10.1016/j.palaeo.2019.109294

van de Schootbrugge, B., McArthur, J. M., Bailey, T. R., Rosenthal, Y., Wright, J. D., & Miller, K. G. (2005). Toarcian oceanic anoxic event: An assessment of global causes using belemnite C isotope records. *Paleoceanography*, *20*(3). https://doi.org/10.1029/2004pa001102

Wang, D., Ling, H. F., Struck, U., Zhu, X. K., Zhu, M., He, T., et al. (2018). Coupling of ocean redox and animal evolution during the Ediacaran-Cambrian transition. *Nature Communications*, *9*, 2575. https://doi.org/10.1038/s41467-018-04980-5

Wang, Y., Ossa Ossa, F., Wille, M., Schurr, S., Saussele, M., Schmid-Röhl, A., & Schoenberg, R. (2020). Evidence for local carbon-cycle perturbations superimposed on the Toarcian carbon isotope excursion. *Geobiology*, *18*, 682–709. https://doi.org/10.1111/gbi.12410

Zhang, X., Sigman, D. M., Morel, F. M. M., & Kraepiel, A. M. L. (2014). Nitrogen isotope fractionation by alternative nitrogenases and past ocean anoxia. *Proceedings of the National Academy of Sciences*, *111*(13), 4782–4787. https://doi.org/10.1073/pnas.1402976111

Ziegler, P. A. (1988). Evolution of the Arctic-North Atlantic and the Western Tethys. *AAPG Memoir. 43*, 198.